ACS OMEGA

Open Access

http://pubs.acs.org/journal/acsodf

Article

Comparative Evaluation of Pyrrole Fused Donor Moieties: 1H-Indole and Pyrrolo[2,3-*b*] Pyridine in Benzothiadiazole-Based D−A−D Type Conjugated Small Molecules for Organic Field-Effect Transistors

Chinthaka M. Udamulle Gedara,[†] Ashutosh Shrivastava,[†] Ziyuan Ma, Prabhath L. Gamage, Chandima Bulumulla, Dushanthi S. Dissanayake, Md Muktadir Talukder, Mihaela C. Stefan, and Michael C. Biewer*

Cite This: *ACS Omega* 2025, 10, 12357−12365

Read Online

ACCESS | Metrics & More | Article Recommendations | Supporting Information

ABSTRACT: Pyrrolic units have been utilized as building blocks for organic semiconducting small molecules and polymers in the recent past. Even though pyrrole-based materials have shown promising semiconducting properties, they have been challenging due to their lower stability under ambient conditions. In this study, we synthesized two pyrrole-fused moieties: 1*H*-indole (IN) and pyrrolo[2,3-*b*] pyridine (PPy), which were then explored for their potential as effective donor moieties in organic semiconducting materials. Each donor block was employed to synthesize two donor−acceptor−donor-type small molecules. Thiophene-flanked benzo[*c*][1,2,5]thiadiazole was used as an acceptor to generate diethyl 6,6'-(benzo[*c*][1,2,5]thiadiazole-4,7-diylbis(thiophene-5,2-diyl))bis(1-dodecyl-1H-indole-2-carboxylate (**IN-BT2T-IN**) and diethyl 6,6'-(benzo[c][1,2,5]thiadiazole-4,7-diylbis(thiophene-5,2-diyl))bis(1-dodecyl-1H-pyrrolo[2,3-*b*]pyridine-2-carboxylate (**PPy-BT2T-PPy**) donor−acceptor−donor molecules. These novel donor−acceptor−donor molecules were tested for their hole-transport properties by fabricating and testing organic field-effect transistors (OFETs). Both molecules exhibited moderate hole-transporting properties with maximum hole mobilities of 0.00483 and 0.00381 $cm^2\ V^{-1}\ s^{-1}$ for **IN-BT2T-IN** and **PPy-BT2T-PPy**, measured under annealing conditions. The enhanced hole mobilities measured in the annealed OFET devices were attributed to thermally induced crystallinity, as demonstrated by atomic force microscopy and grazing incidence X-ray diffraction measurements.

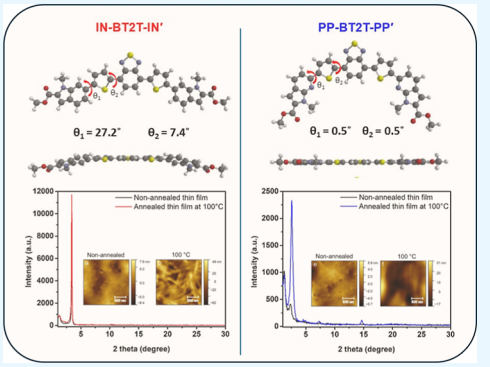

INTRODUCTION

Solution-processable organic semiconducting materials have gained popularity due to several advantages: low-cost processing, large-area applicability, mechanical flexibility, and reasonably high charge carrier mobilities (>1 $cm^2\ V^{-1}\ s^{-1}$).[1,2] Solvent-processable organic semiconducting polymers have achieved hole mobilities that exceed those of amorphous silicon (0.1−1.0 $cm^2\ V^{-1}\ s^{-1}$)[3−5] and approach those of polycrystalline silicon (>10 $cm^2\ V^{-1}\ s^{-1}$)[6−8] in organic field-effect transistors (OFETs). On the other hand, hole mobilities extracted from semiconducting small-molecule-containing devices are behind their polymeric counterparts.[9] Thus, there is still plenty of opportunity to explore new small molecule designs and donor blocks to further our understanding of structure−property relationships that play a vital role in OFET performance.

Pyrrole is an important structural moiety, as it possesses a greater electron density than its isoelectronic five-membered aromatic rings, such as thiophene, furan, and selenophene. This characteristic provides it with better donor properties and the potential to be utilized in solution-processable organic electronics.[10,11] Pyrrole and its derivatives serve as key structural motifs of functional materials applied in various fields such as pharmaceuticals, polymer chemistry, natural product synthesis, biomedical engineering, and photochromism.[12,13] Pyrrole-based materials exhibit excellent semiconducting properties and have been studied for applications in OFETs and organic photovoltaics (OPVs).[11,14] Despite their promising donor properties, pyrrole systems are comparatively understudied due to challenges in synthesis, particularly their lower stability in ambient conditions due to high electron density.[15−17]

Organic polymers with longer conjugation lengths and good film-forming ability are desirable for large-area applications,[18−24] but charge carrier mobilities often depend on

Received: December 17, 2024
Revised: March 3, 2025
Accepted: March 11, 2025
Published: March 19, 2025

Scheme 1. General Synthesis Route for IN-BT2T-IN and PPy-BT2T-PPy; Reaction Conditions: (a) Ethyl Azidoacetate (2 equiv), Ethyl Trifluoroacetate (2 equiv), Metal−Sodium (2 equiv), Ethanol, 0 °C, 6 h; (b) Toluene, Reflux, 24 h; (c) Anhydrous K_2CO_3 (2.1 equiv), 18-Crown-6 (cat.), 1-Bromododecane (2 equiv), Dimethylformamide, 120 °C, 24 h, N_2; (d) Trimethyl(thiophen-2-yl)stannane (2.2 equiv), $Pd_2(dba)_3$ (3 mol %), P(*p*-tol)$_3$ (12 mol %), Toluene, Reflux, 12 h; (e−i) *n*-BuLi (> 2 equiv), Tetrahydrofuran (THF), −78 °C, 1 h: (ii) Trimethylstannylchloride (> 2 equiv), THF, −78 °C, 3 h, RT; (f) [11] (1 equiv), [7] or [8] (2.2 equiv), $Pd_2(dba)_3$ (10 mol %), P(*p*-tol)$_3$ (40 mol %), Toluene, Reflux, 24 h

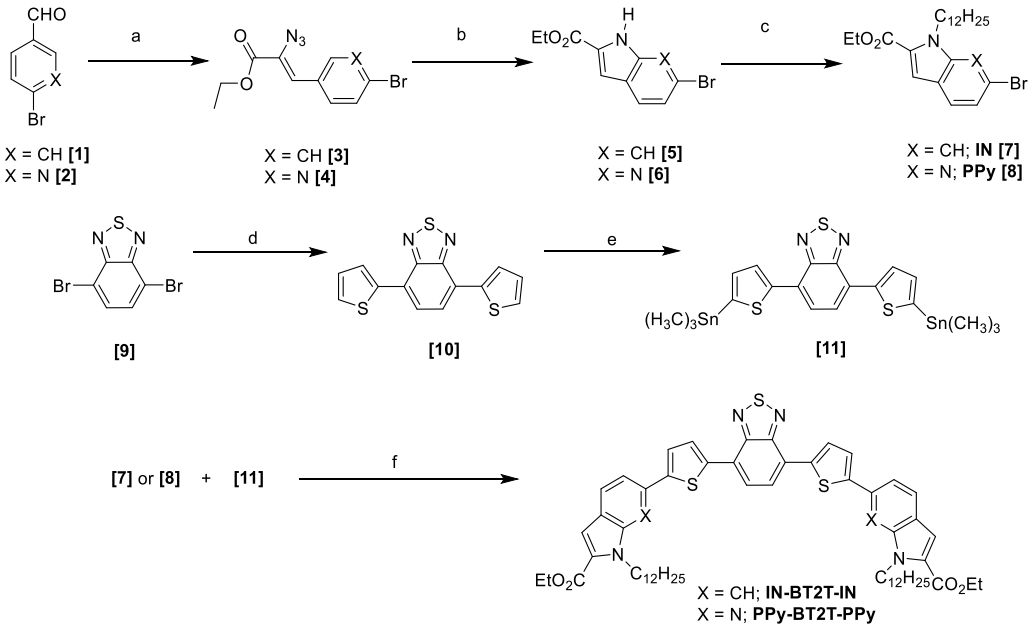

molecular weights.[25−29] The irreproducible molecular weights and broad molecular weight distribution can lead to batch-to-batch variations in the OFET performance.[30] In contrast, organic semiconducting small molecules exhibit well-defined molecular weights and orderly crystal packing arrangements, which helps in minimizing variations that usually occur in polymers due to inter or intrachain interactions, variable chain lengths, and conformational complexities that might introduce energetic disorders.[31,32] Hence, these small molecules have gained attention in solution-processable organic electronics for their high purities, well-defined structures, precise molecular weights, and high degree of order.[33−36]

The ability to achieve more reproducible results with small molecules has enabled further improvements in OFETs' properties, such as charge-carrier mobility, making them more competitive with polymers. So far, high-performing organic small molecules often rely on vacuum deposition techniques, which require ultrahigh vacuum conditions.[37−39] These methods pose practical difficulties and limit their cost-effectiveness, making real-world applications more challenging. For these molecules, the requirement for vacuum deposition arises from the absence of solubilizing alkyl chains, which are insulating by nature. Thus, designing solution-processable small molecules without compromising charge carrier mobility remains a significant challenge.

High-performing solution-processable small molecules, in most cases, comprise donor−acceptor (D−A) architecture involving acenes or heterocyclic fused ring systems.[39−43] Fused ring systems are relatively more stable than individual aromatic rings due to their low-lying highest occupied molecular orbital (HOMO) energy levels, resulting from conjugated resonance stabilization, and they provide larger $\pi-\pi$ overlapping areas that assist charge transport through the hopping mechanism.[5,18,44] Commonly used fused ring systems in organic electronics include thieno[3,2-*b*]thiophene (TT),[5,18,19] dithieno[3,2-*b*:2′,3′-*d*]pyrroles (DTP),[31,45] thieno[3,2-*b*]-pyrrole (TP),[32,46−48] dithienosilole,[36,49] selenopheno[3,2-*b*]-pyrrole,[9,50] and cyclopentadithiophene.[51] Designing pyrrole-based organic small molecules fused with other stable aromatic rings produces relatively ambient-stable donors.[9] Compared with DTP and TP units, other pyrrole fused-ring systems have received inadequate attention as potential candidates for OFET materials.

Recently, our group published several donor−acceptor−donor (DAD)-type small molecules featuring relatively understudied TP donors and benzo[*c*][1,2,5]thiadiazole (BT) acceptor units connected through various spacers, such as thiophene,[32,46] furan,[32,52] bithiophene, and TT.[46] Some of these molecules demonstrated hole mobilities ranging from 1 × 10^{-1} to 1 × 10^{-2} cm^2 V^{-1} s^{-1}. Following a similar approach, our current focus is to investigate more versatile nonconventional pyrrole-fused ring systems comparable with TP to better understand the structure−property relationships in fused-pyrroles for OFET's applications. 1*H*-indole (IN) and pyrrolo[2,3-*b*] pyridine (PPy) are pyrrole-based fused ring systems that have not been extensively studied in the context of OFET materials. IN units have been reported in a few squaric-acid-pyrrole-based conjugated polymers applied in OPVs (OPV).[53] However, to the best of our knowledge, PPy has not yet been reported in organic electronics and related applications. Thus, in this study, IN and PPy donor systems were combined with a BT acceptor via thiophene spacers and their optoelectronic potential was investigated by comparing their HOMO/lowest unoccupied molecular orbital (LUMO) levels with TP using density functional theoretical (DFT) (B3LYP/6-31G*; see Figure S24). Based on the comparable results obtained, we synthesized and characterized two BT-based small molecules containing ester-monocapped 1*H*-indole

https://doi.org/10.1021/acsomega.4c11362
ACS Omega 2025, 10, 12357−12365

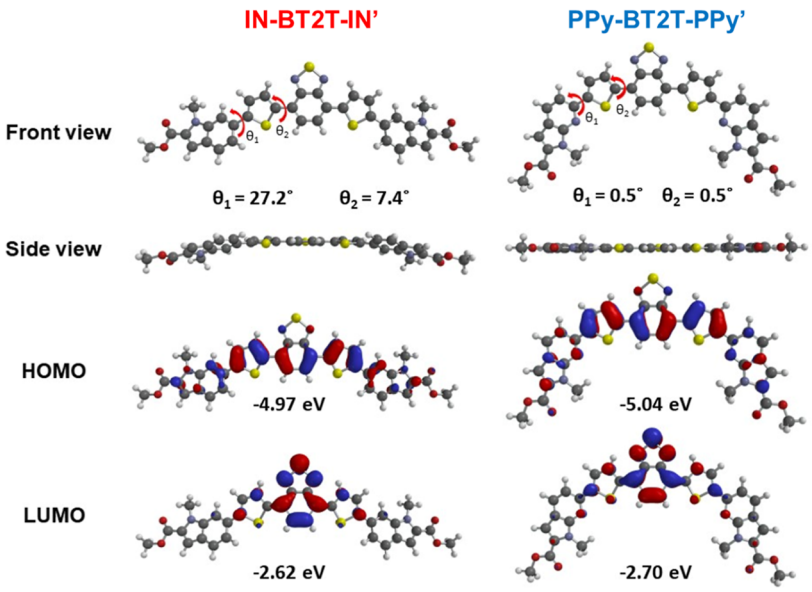

Figure 1. DFT analysis of small molecules was performed to predict HOMO−LUMO energies and molecular planarity.

(IN) and pyrrolo[2,3-*b*] pyridine (PPy) donors, as illustrated in Scheme 1. This study aims to elucidate the structure-property relationship of the suggested fused-pyrrole donor blocks in BT-acceptor-based D−A−D semiconducting small molecules and assess their potential for OFET applications.

RESULTS AND DISCUSSION

DFT Calculations. Conformational calculations were performed for both **IN-BT2T-IN** and **PPy-BT2T-PPy** backbones at the B3LYP/6-31G* level of theory and basis set using Spartan'16 software to predict HOMO/LUMO energy levels and energy-minimized conformations. Dodecyl- and ethyl alkyl chains were replaced with methyl groups to obtain **IN-BT2T-IN′** and **PPy-BT2T-PPy′**, thereby avoiding complexity due to the long flexible chain that significantly reduces computing power and time spent during the calculations. Optimized geometries, HOMO−LUMO energies, and frontier molecular orbitals are listed in Figure 1. Both molecules exhibit nearly planar backbones in their energy-minimized geometries. **IN-BT2T-IN′** showed a relatively larger dihedral angle between the IN and thiophene blocks (27.2°) due to possible repulsive interactions between spatially closer hydrogen atoms on each block facing each other. The dihedral angle between the BT and thiophene spacer showed a relatively lower value (7.4°). In contrast, **PPy-BT2T-PPy′** exhibits almost zero dihedral angles (≈0.5°) between all the major counterparts, leading to nearly perfect backbone planarity.

Introducing PPy into the **PPy-BT2T-PPy′** structure, compared to **IN-BT2T-IN′**, leads to the formation of additional S−N intramolecular interactions between the C−S antibonding orbitals in thiophene and the lone pair on the pyridinic nitrogen atom in PPy.[54] Additionally, the shorter pyridinic C−N bond (1.33 Å) in PPy compared to the benzoic C−C (1.40 Å) bond in IN results in a further curved backbone, which increases the distance between the hydrogen atoms of PPy and thiophene units on the same plane, thereby eliminating repulsive interactions. When considering the HOMO−LUMO orbital distribution, in both small molecules, the LUMO is only delocalized in the core BT2T unit, while the HOMO is delocalized along the entire backbone. For both molecules, the corresponding calculated HOMO and LUMO energy values showed no significant difference.

The synthesis of **IN-BT2T-IN** and **PPy-BT2T-PPy** is shown in Scheme 1. Briefly, commercially purchased 4-bromo benzaldehyde [1] and 6-bromonicotinaldehyde [2] were subjected to Knoevenagel condensation with ethyl azidoacetate, using ethyl trifluoroacetate as a "sacrificial electrophile" and sodium ethanolate as the base to synthesize their corresponding acrylates [3] and [4], respectively. The resulting acrylates were then converted into ethyl 6-bromo-1*H*-indole-2-carboxylate [5] and ethyl 6-bromo-1*H*-pyrrolo[2,3-*b*] pyridine-2-carboxylate [6], respectively, by employing Hemetsberger cyclization in toluene. The cyclized products [5] and [6] then underwent *N*-alkylation steps, where the deprotonation of pyrrolic hydrogens with K_2CO_3 followed by addition of 1-bromododecane to yield pyrrolic monomers, ethyl 6-bromo-1-dodecyl-1*H*-indole-2-carboxylate [7] and ethyl 6-bromo-1-dodecyl-1H-pyrrolo[2,3-*b*] pyridine-2-carboxylate [8]. BT2T [10] was synthesized via a Stille coupling reaction between 4,7-dibromobenzo[c][1,2,5]thiadiazole [9] and trimethyl-(thiophen-2-yl)stannane. BT2T [10] was later employed in the stannylation step by the addition of *n*-BuLi at −78 °C, followed by trimethylstannyl chloride solution to produce the acceptor block 4,7-bis(5-(trimethylstannyl)thiophen-2-yl)-benzo[c][1,2,5]thiadiazole [11]. **IN-BT2T-IN** and **PPy-BT2T-PPy** were then synthesized through a Stille coupling reaction between [11] and [7] or [8], respectively, in the presence of a tris(dibenzylideneacetone)dipalladium (0) catalyst and tri(*o*-tolyl)phosphine ligand. Detailed experimental procedures are provided in the Supporting Information. The synthesized compounds were characterized with ^{1}H and ^{13}C NMR, as well as matrix-assisted laser desorption ionization (MALDI) time-of-flight (TOF), which are shown in Figures S1−S23 in the Supporting Information.

UV−vis absorption spectra for the **IN-BT2T-IN** and **PPy-BT2T-PPy** molecules were obtained in thin film and solution (in chloroform). For both small molecules, UV−vis spectra exhibited the typical dual-band nature corresponding to donor−acceptor organic semiconductors. The absorption spectra for both molecules are shown in Figure 2. In solution,

https://doi.org/10.1021/acsomega.4c11362
ACS Omega 2025, 10, 12357−12365

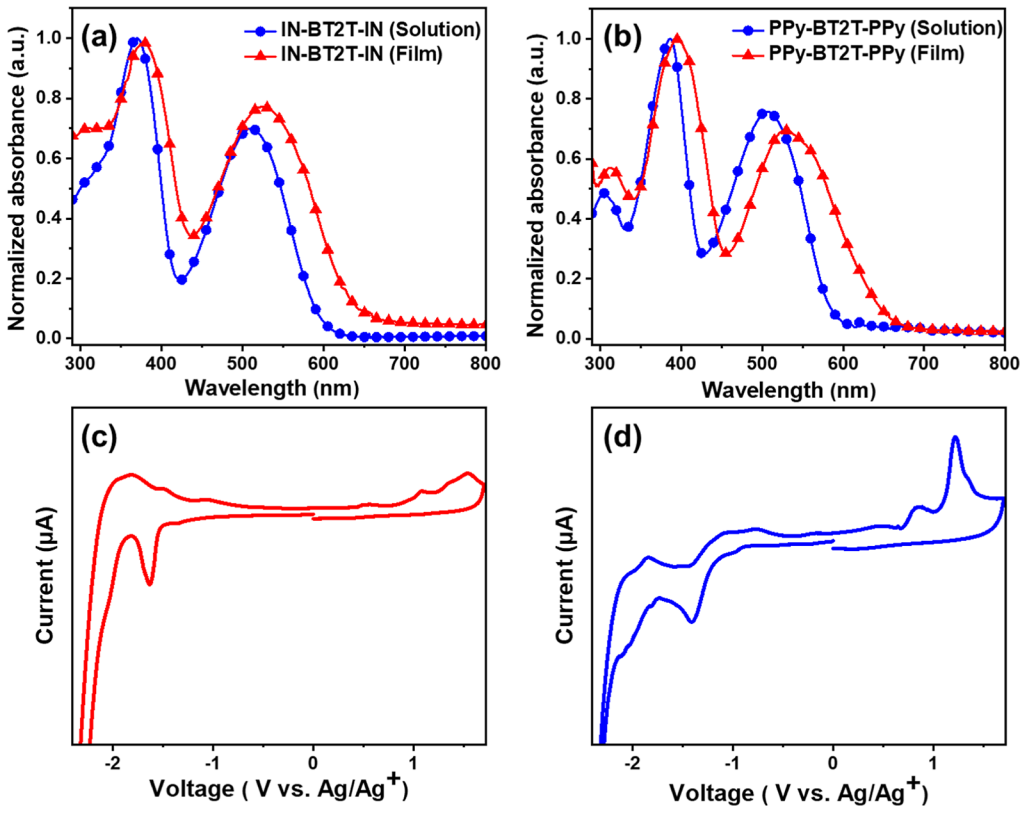

Figure 2. UV−vis spectra of small molecules: (a) **IN-BT2T-IN** and (b) **PPy-BT2T-PPy**; cyclic voltammogram of small molecules: (c) **IN-BT2T-IN** and (d) **PPy-BT2T-PPy**.

Table 1. Optical and Electrochemical Properties of IN-BT2T-IN and PPy-BT2T-PPy

small molecule	E_{HOMO} [a] (eV)	E_{LUMO} [b] (eV)	E_g^{ec} (eV)	E_g^{opt} (eV)	λ_{max}^{sol} (nm)	λ_{max}^{film} (nm)	λ_{onset} (nm)
IN-BT2T-IN	−4.83	−2.86	1.97	1.97	369, 510	379, 525	629
PPy-BT2T-PPy	−5.10	−3.19	1.92	1.91	386, 507	395, 528	650

[a]The HOMO energy was calculated using formula: $E_{HOMO} = -(E_{ox} + 4.4)$ eV. [b]The LUMO energy was calculated using formula: $E_{LUMO} = -(E_{red} + 4.4)$ eV.

higher energy bands appeared with absorption maxima at 369 nm (**IN-BT2T-IN**) and 386 nm (**PPy-BT2T-PPy**), corresponding to $\pi-\pi^*$ transitions. Lower energy bands, corresponding to intramolecular charge transfer from the backbone-delocalized HOMO to the acceptor-centered LUMO, as depicted by DFT, appeared with peak maxima at 510 nm for **IN-BT2T-IN** and 507 nm for **PPy-BT2T-PPy**. Compared to **IN-BT2T-IN**, **PPy-BT2T-PPy** exhibited a slight red shift (17 nm) in the low-energy band, while no significant difference in the peak position was observed for the high-energy band. In thin films, both small molecules showed bathochromic shifts in both characteristic bands, with the high energy bands appearing at an absorption maxima of 379 nm (**IN-BT2T-IN**) and 395 nm (**PPy-BT2T-PPy**). In comparison, the charge-transfer bands appeared with maxima at 525 nm (**IN-BT2T-IN**) and 528 nm (**PPy-BT2T-PPy**). When comparing the thin-film spectra with the solution-based spectra, the high energy bands showed a slight red shift of approximately 10 nm for both small molecules, whereas the charge-transfer bands displayed red shifts of 15 and 21 nm for **IN-BT2T-IN** and **PPy-BT2T-PPy**, respectively. These results indicate that the red shifts occur in the film absorption spectra of both small molecules compared to the solution due to enhanced intermolecular interactions between the molecules in the thin film relative to the solution. The optical band gaps (E_g^{opt}) for **IN-BT2T-IN** and **PPy-BT2T-PPy** were calculated to be 1.97 and 1.91 eV, respectively, using the onset of the charge-transfer band in the absorption profile for both small molecules.

Cyclic voltammetry (CV) was used to determine the electrochemical band gap (E_g^{ec}) and HOMO/LUMO energies (Figure 2c,d). For this purpose, a thin film of the samples was deposited on the working electrode of the three-electrode setup, and onset potentials of the oxidation and reduction peaks (E_{ox} and E_{red}) in the voltammogram were used to calculate the HOMO and LUMO energy levels, respectively. The HOMO/LUMO energies for **IN-BT2T-IN** and **PPy-BT2T-PPy** were found to be −4.83/−2.86 and −5.10/−3.19 eV, resulting in calculated electrochemical band gaps of 1.97 and 1.91 eV, respectively.

Relatively deeper-lying HOMO and LUMO levels were observed for **PPy-BT2T-PPy**, likely due to the more electronegative additional nitrogen atom present in the fused-pyridine ring of the PPy compared to the IN moieties in **IN-BT2T-IN**. Surprisingly, no significant discrepancy between E_g^{opt} and E_g^{ec} was observed for both small molecules, which is typically noted due to the associated exciton binding energy. However, both small molecules showed E_g^{ec} comparable to the observed E_g^{ec} (=1.90 eV) for thiophene-based

https://doi.org/10.1021/acsomega.4c11362
ACS Omega 2025, 10, 12357−12365

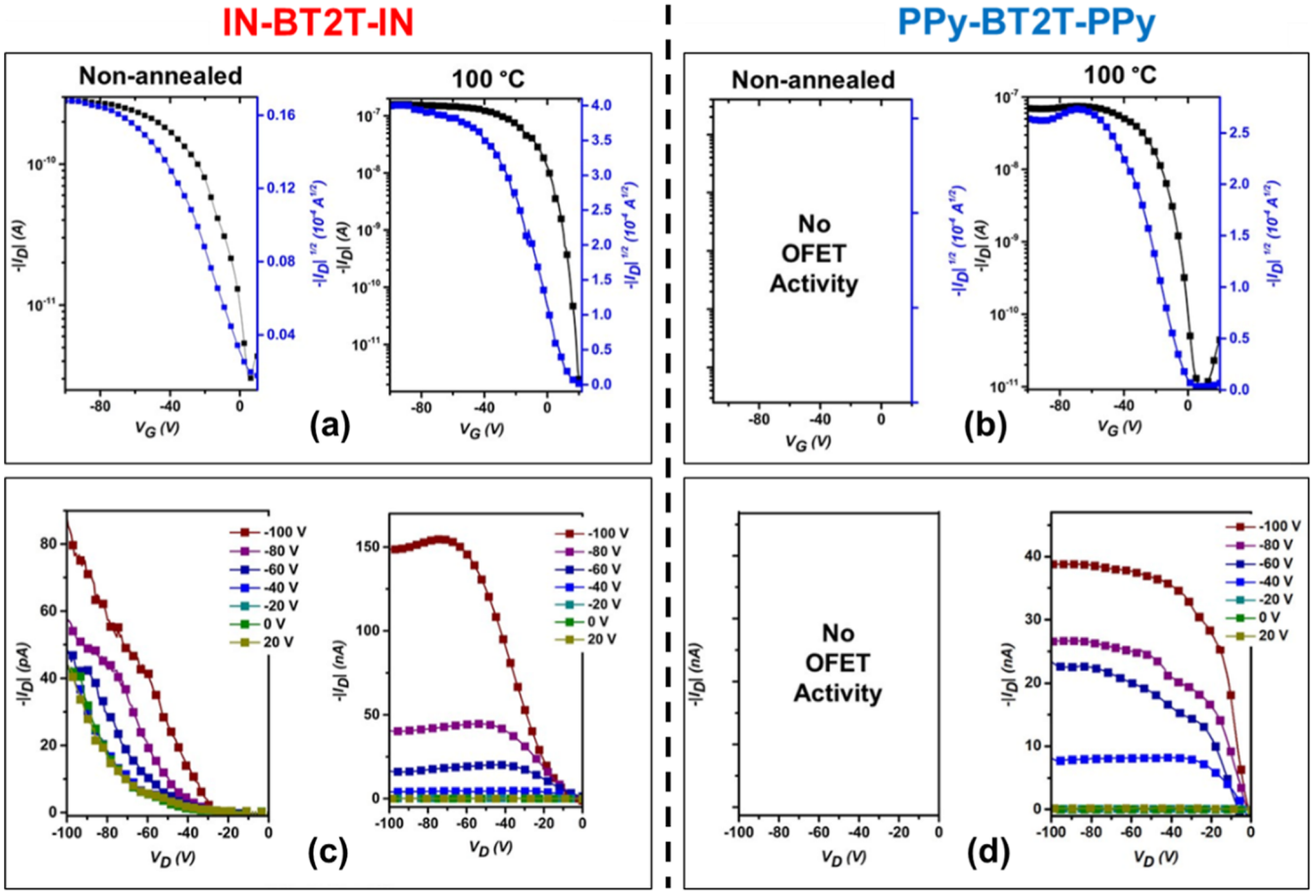

Figure 3. OFET transfer curves of (a) **IN-BT2T-IN** and (b) **PPy-BT2T-PPy** at nonannealed and annealed (at 100 °C) devices; OFET output curves of (c) **IN-BT2T-IN**, and (d) **PPy-BT2T-PPy** at nonannealed and annealed (at 100 °C) devices.

analogues (TP-BT2T-TP) in the literature.[32] TP-BT2T-TP indicates a slightly elevated HOMO compared to **IN-BT2T-IN**, attributed to the presence of relatively electron-rich fused thiophene in TP-BT2T-TP. Meanwhile, **PPy-BT2T-PPy** exhibited a significantly deeper-lying HOMO compared with the other two small molecules mentioned above. This significant change is due to an electron-withdrawing sp^2-hybridized nitrogen atom in the fused-pyridine moiety. The important parameters for optical and electrochemical properties obtained from UV−vis spectroscopy and CV are summarized in Table 1.

The thermal stability and phase transitions, including any thermal transitions of the small molecules, were studied by using thermogravimetric analysis (TGA) and differential scanning calorimetry (DSC) techniques, respectively. The corresponding TGA and DSC curves are shown in Figure S25. TGA results indicate reasonable thermal stability in both small molecules, with decomposition temperatures (T_d, 5% weight loss) at ∼ 338 °C for **IN-BT2T-IN** and ∼ 395 °C for **PPy-BT2T-PPy**.

However, **IN-BT2T-IN** showed relatively lower thermal stability, while **PPy-BT2T-PPy** exhibited similar stability compared with the previously reported TP-BT2T-TP (T_d = 385 °C). DSC experiments were performed to acquire additional thermal events such as phase transition or melting temperatures. For both small molecules, sharp first-order melting temperatures (T_m) were observed at ∼ 125 °C (**IN-BT2T-IN**) and ∼ 116 °C (**PPy-BT2T-PPy**). A first-order crystallization temperature (T_c) was observed only for **PPy-BT2T-PPy** at ∼47 °C in the cooling curves, whereas **IN-BT2T-IN** did not show any first-order crystallization exothermic peak until 25 °C in the cooling cycle.

OFET parameters were obtained using a bottom-gate/bottom-contact (BGBC) device configuration (Figure 3). For nonannealed thin films, **PPy-BT2T-PPy** showed no significant OFET activity, while **IN-BT2T-IN** demonstrated an average hole mobility of 4.85×10^{-5} cm^2 V^{-1} s^{-1}, with a maximum of 1.12×10^{-4} cm^2 V^{-1} s^{-1}. After annealing at 100 °C, both the small molecules exhibited similar average hole mobilities, with maximum hole mobilities of 4.83×10^{-3} and 3.81×10^{-3} cm^2 V^{-1} s^{-1}, respectively, for **IN-BT2T-IN** and **PPy-BT2T-PPy**. Thermal annealing at different temperatures indicated a gradual increase in hole mobility as the temperature increased until 100 °C for **IN-BT2T-IN** and **PPy-BT2T-PPy**. A similar trend was previously observed for TP-BT2T-TP, as reported by our group.[32] We further annealed above 100 °C and observed that the thin film started deteriorating. This was primarily due to the melting of the thin film, which can be attributed to its melting temperature being close to 110−125 °C, as indicated by DSC analysis for both molecules. Consequently, it was impossible to perform OFET testing at temperatures above 100 °C. Even at 110 °C, the thin films were visibly observed to melt, further confirming the thin films' thermal instability at elevated temperatures.

Both molecular semiconducting devices significantly changed the on−off current ratio ($I_{on/off}$) upon thermal

https://doi.org/10.1021/acsomega.4c11362
ACS Omega 2025, 10, 12357−12365

Table 2. OFET Parameters Obtained from BGBC Configuration

small molecule	annealing temperature/ °C	maximum hole mobility/cm^2 V^{-1} s^{-1}	[a]average hole mobility (μ_h)/cm^2 V^{-1} s^{-1}	threshold voltage	on/off current ratio
IN-BT2T-IN	nonannealed	1.12×10^{-4}	4.85×10^{-5}	(−2.1) − 11.0 V	10^2
	60	8.90×10^{-4}	4.67×10^{-4}	(−6.9) − 4.5 V	10^3 to 10^4
	100	4.83×10^{-3}	2.61×10^{-3}	(−1.2) − 13.4 V	10^5 to 10^6
PPy-BT2T-PPy	nonannealed				
	60	4.48×10^{-4}	9.84×10^{-5}	10.6−15.9 V	10^2 to 10^3
	100	3.81×10^{-3}	2.33×10^{-3}	11.7−22.2 V	10^4 to 10^5
TP-BT2T-TP[32]	nonannealed	3.88×10^{-5}	2.76×10^{-5}	−0.5−0.5 V	$>10^1$
	60	5.98×10^{-5}	2.76×10^{-5}	−2.5−1.0 V	$>10^2$
	100	4.27×10^{-2}	3.86×10^{-2}	−3.0 − −1.5 V	$>10^4$

[a]Calculated hole mobilities were extracted from 6 individual devices.

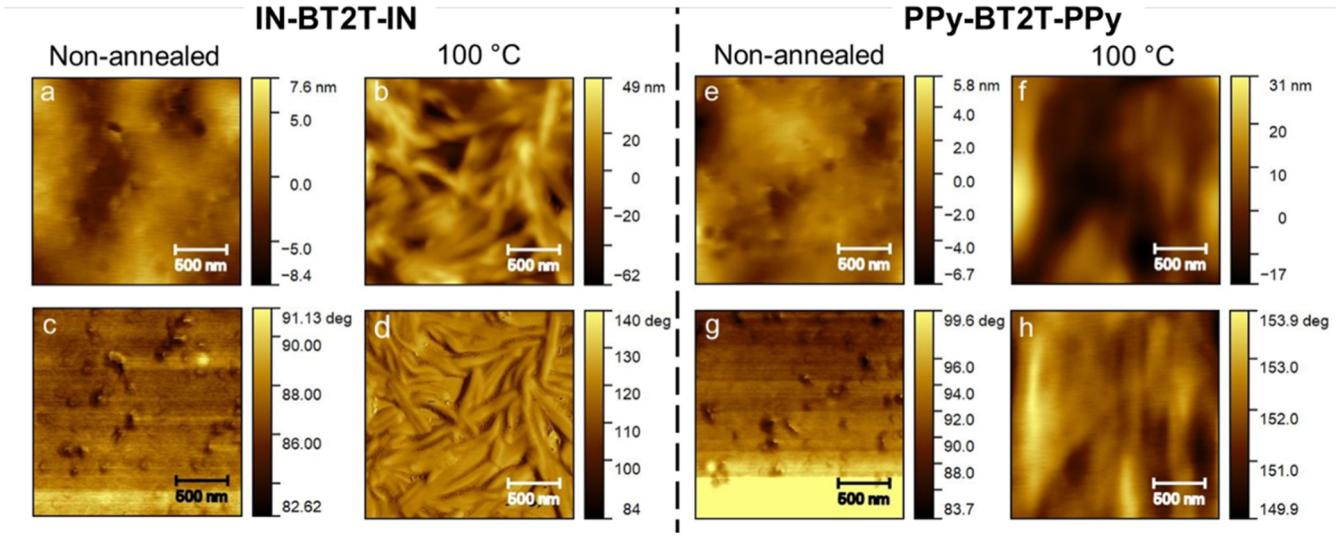

Figure 4. Height (top) and phase (bottom) images of **IN-BT2T-IN** (left-half) and **PPy-BT2T-PPy** (right-half) for nonannealed (a,c and e,g) and annealed thin films at 100 °C (b,d and f,h), obtained from TMAFM; scale bar indicates 500 nm length.

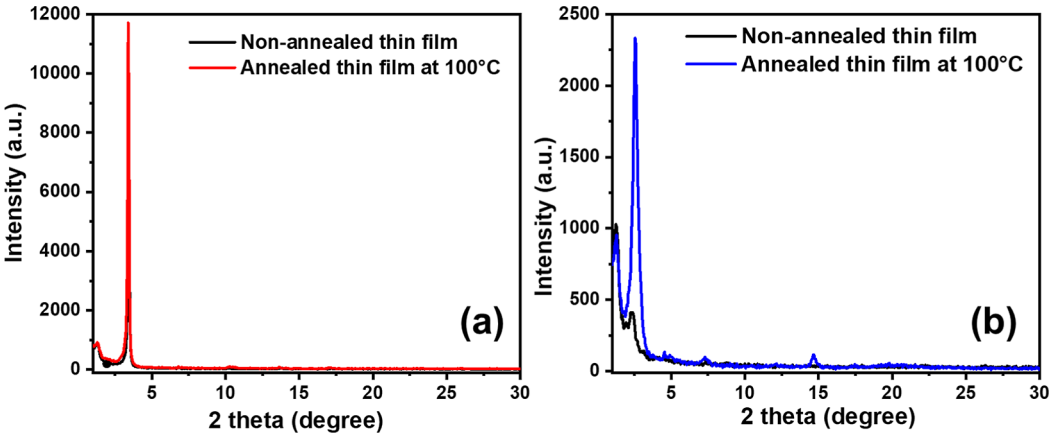

Figure 5. GIXRD spectra of (a) **IN-BT2T-IN** and (b) **PPy-BT2T-PPy** for nonannealed and annealed (at 100 °C) thin films on the OTMS-modified silicon substrate.

annealing. The $I_{on/off}$ ratio changed from 10^2 to 10^6 for **IN-BT2T-IN** and from 10^2 to 10^5 for **PPy-BT2T-PPy**. **IN-BT2T-IN** showed threshold voltages (V_T) varying from negative to positive values, while **PPy-BT2T-PPy** remained positive for all annealing temperatures. All of the OFET parameters are summarized in Table 2.

Tapping mode atomic force microscopy analysis was performed to understand the surface morphology changes upon thermal annealing. Both **IN-BT2T-IN** and **PPy-BT2T-PPy** exhibited smoother morphologies for nonannealed thin films, with root-mean-square roughness (RMS) values of 2.10 and 1.41 nm, respectively.

Upon annealing at 100 °C, the roughness of the thin-film surface increased for each material, showing RMS values of 16.96 and 8.78 nm, respectively (see Figure 4b,f). In comparison, TP-BT2T-TP reported in the literature showed

https://doi.org/10.1021/acsomega.4c11362
ACS Omega 2025, 10, 12357−12365

an RMS value of 7.24 nm with the improved granular morphology for annealed thin films. **IN-BT2T-IN** exhibited a fibrillar nature (Figure 4b,d), contributing to a greater roughness in the surface morphology compared to **PPy-BT2T-PPy**, which displayed a grainy morphology at an annealing temperature of 100 °C (Figure 4f,h). Both fibrillar and grainy morphologies indicated better aggregation of small molecules with reduced molecular distances, leading to significantly larger crystallites. These morphological changes correspond to the enhanced hole mobilities in each material upon thermal annealing.

A grazing incidence X-ray diffraction (GIXRD) experiment was conducted to further study the structural changes in the thin films. The parameters calculated from the (100) diffraction peak showed that **IN-BT2T-IN** has a considerably lower *d*-spacing (see Table S1). While **IN-BT2T-IN** exhibited no significant change in lamellar packing distances upon annealing, **PPy-BT2T-PPy** showed a reduction of 3.8 Å. Initially, **PPy-BT2T-PPy** displayed a low-intensity peak that was significantly enhanced upon annealing, indicating an apparent increase in the crystallinity of the thin film. This observation aligns with the notable improvement in hole mobility in **PPy-BT2T-PPy** OFETs when annealed to 100 °C, increasing from no measurable hole mobility to a magnitude of 1×10^{-3} cm^2 V^{-1} s^{-1}. The relatively broad (100) diffraction peak of **PPy-BT2T-PPy** (Figure 5b) indicates the presence of smaller out-of-plane crystallites in the thin film compared to those in **IN-BT2T-IN**, which could be attributed to the relatively large out-of-plane lamellar *d*-spacing values of **PPy-BT2T-PPy**. In comparison, the lamellar packing distance calculated from the (100) peak for TP-BT2T-TP has shown a moderate value (30.96 Å) relative to the two molecules studied in this case. Additionally, TP-BT2T-TP exhibited several orders of Bragg's reflection peaks, indicating the highly ordered nature of the films.[32] The hole mobility of **PPy-BT2T-PPy** is lower at 60 and 100 °C compared to **IN-BT2T-IN**, which can be attributed to differences in the degree of crystallinity. Although both molecules exhibit increased crystallinity upon annealing, the degree of crystallinity varies, as shown in Figure 5. The intensity observed for **IN-BT2T-IN** is significantly higher than that for **PPy-BT2T-PPy** when annealed at 100 °C (see Table S1 in the Supporting Information). The lower degree of crystallinity of **PPy-BT2T-PPy** may result in weaker intermolecular interactions at elevated temperatures compared to that of **IN-BT2T-IN**, thereby hindering efficient charge transport.

CONCLUSIONS

In summary, the synthesis of two novel donor−acceptor−donor semiconducting small molecules containing fused-pyrrole ring systems, IN and PPy, was accomplished, and they were characterized for their purity and optoelectronic, thermal, and OFET properties. DFT calculations showed greater planarity in **PPy-BT2T-PPy** than in **IN-BT2T-IN**, possibly due to the intramolecular S−N interactions between the PPy donor and the spacer thiophene, which reduce the torsion angle through conformational locking. Despite the difference in backbone planarity, both small molecules showed optoelectronic properties comparable to those of similar electrochemical and optical band gaps. The minimal difference between the electrochemical and optical band gaps for both molecules indicates ease of charge injection at the thin-film electrode interface during the CV measurements. Both small molecules demonstrated significant thermal stability with degradation temperatures exceeding 200 °C. The OFET properties seemed comparable at optimized annealing conditions of each small molecule in this study, aligning with their similar optoelectronic properties. However, surface morphology studies showed an increased crystallinity in the annealed thin films compared to the nonannealed ones, which is also well supported by GIXRD data in this study. The thermally induced crystallinity of thin films under optimized annealing conditions helped to improve intermolecular interactions, enhancing hole mobility in both materials. Despite the planarity differences observed in the DFT results, both small molecules exhibited comparable optoelectronic properties, indicating similar effective conjugation and stacking properties. This study will contribute to establishing a structure−property relationship that will ultimately aid in designing novel semiconducting small molecules with the desired optoelectronic properties for various organic electronic applications.

ASSOCIATED CONTENT

Supporting Information

The Supporting Information is available free of charge at https://pubs.acs.org/doi/10.1021/acsomega.4c11362.

Materials and experimental methods, synthetic procedures, ^{1}H and ^{13}C NMR spectra, TGA, DSC, MALDI-TOF spectra, and DFT calculation (PDF)

AUTHOR INFORMATION

Corresponding Author

Michael C. Biewer − *The Department of Chemistry and Biochemistry, The University of Texas at Dallas, Richardson, Texas 75080-3021, United States;* orcid.org/0000-0001-5249-6341; Email: biewerm@utdallas.edu

Authors

Chinthaka M. Udamulle Gedara − *The Department of Chemistry and Biochemistry, The University of Texas at Dallas, Richardson, Texas 75080-3021, United States*

Ashutosh Shrivastava − *The Department of Chemistry and Biochemistry, The University of Texas at Dallas, Richardson, Texas 75080-3021, United States;* orcid.org/0000-0002-5348-1376

Ziyuan Ma − *The Department of Chemistry and Biochemistry, The University of Texas at Dallas, Richardson, Texas 75080-3021, United States*

Prabhath L. Gamage − *The Department of Chemistry and Biochemistry, The University of Texas at Dallas, Richardson, Texas 75080-3021, United States*

Chandima Bulumulla − *The Department of Chemistry and Biochemistry, The University of Texas at Dallas, Richardson, Texas 75080-3021, United States;* Present Address: HHMI Janelia Research Campus, 19700 Helix Drive, Ashburn, VA, 20147, US

Dushanthi S. Dissanayake − *The Department of Chemistry and Biochemistry, The University of Texas at Dallas, Richardson, Texas 75080-3021, United States;* orcid.org/0000-0002-1974-3467

Md Muktadir Talukder − *The Department of Chemistry and Biochemistry, The University of Texas at Dallas, Richardson, Texas 75080-3021, United States*

https://doi.org/10.1021/acsomega.4c11362
ACS Omega 2025, 10, 12357−12365

Mihaela C. Stefan − *The Department of Chemistry and Biochemistry, The University of Texas at Dallas, Richardson, Texas 75080-3021, United States;* orcid.org/0000-0003-2475-4635

Complete contact information is available at: https://pubs.acs.org/10.1021/acsomega.4c11362

Author Contributions

†C.M.U.G and A.S. authors contributed equally and should be considered cofirst authors.

Notes

The authors declare no competing financial interest.

■ ACKNOWLEDGMENTS

The author, M.C.S., greatly acknowledges the financial support provided by the National Science Foundation (CHE-1609880 and CHE-1566059) and Welch Foundation (AT1740). M.C.S. thanks the generous endowed chair support from the Eugene McDermott Foundation.

■ REFERENCES

(1) Yang, J.; Zhao, Z.; Wang, S.; Guo, Y.; Liu, Y. Insight into high-performance conjugated polymers for organic field-effect transistors. *Chem.* **2018**, *4* (12), 2748−2785.
(2) Liu, Q.; Bottle, S. E.; Sonar, P. Developments of diketopyrrolopyrrole-dye-based organic semiconductors for a wide range of applications in electronics. *Adv. Mater.* **2020**, *32* (4), 1903882.
(3) Mei, J.; Diao, Y.; Appleton, A. L.; Fang, L.; Bao, Z. Integrated materials design of organic semiconductors for field-effect transistors. *J. Am. Chem. Soc.* **2013**, *135* (18), 6724−6746.
(4) Ong, B. S.; Wu, Y.; Liu, P.; Gardner, S. High-performance semiconducting polythiophenes for organic thin-film transistors. *J. Am. Chem. Soc.* **2004**, *126* (11), 3378−3379.
(5) McCulloch, I.; Heeney, M.; Bailey, C.; Genevicius, K.; MacDonald, I.; Shkunov, M.; Sparrowe, D.; Tierney, S.; Wagner, R.; Zhang, W.; et al. Liquid-crystalline semiconducting polymers with high charge-carrier mobility. *Nat. Mater.* **2006**, *5* (4), 328−333.
(6) Amin, A. Y.; Khassanov, A.; Reuter, K.; Meyer-Friedrichsen, T.; Halik, M. Low-voltage organic field effect transistors with a 2-tridecyl [1] benzothieno [3, 2-b][1] benzothiophene semiconductor layer. *J. Am. Chem. Soc.* **2012**, *134* (40), 16548−16550.
(7) Minemawari, H.; Yamada, T.; Matsui, H.; Tsutsumi, J. y.; Haas, S.; Chiba, R.; Kumai, R.; Hasegawa, T. Inkjet printing of single-crystal films. *Nature* **2011**, *475* (7356), 364−367.
(8) Li, J.; Zhao, Y.; Tan, H. S.; Guo, Y.; Di, C.-A.; Yu, G.; Liu, Y.; Lin, M.; Lim, S. H.; Zhou, Y.; et al. A stable solution-processed polymer semiconductor with record high-mobility for printed transistors. *Sci. Rep.* **2012**, *2* (1), 754.
(9) Ma, Z.; Udamulle Gedara, C. M.; Wang, H.; Biewer, M. C.; Stefan, M. C. Chalcogenopheno [3, 2-b] pyrrole-Containing Donor−Acceptor−Donor Organic Semiconducting Small Molecules for Organic Field-Effect Transistors. *ACS Appl. Mater. Interfaces* **2023**, *15* (39), 46119−46129.
(10) Nogami, Y.; Pouget, J.-P.; Ishiguro, T. Structure of highly conducting PF6−-doped polypyrrole. *Synth. Met.* **1994**, *62* (3), 257−263.
(11) Bulumulla, C.; Gunawardhana, R.; Gamage, P. L.; Miller, J. T.; Kularatne, R. N.; Biewer, M. C.; Stefan, M. C. Pyrrole-containing semiconducting materials: synthesis and applications in organic photovoltaics and organic field-effect transistors. *ACS Appl. Mater. Interfaces* **2020**, *12* (29), 32209−32232.
(12) Kumar S, L.; Servesh, A.; Chundattu, S. J.; Tabassum, S.; Govindaraju, S. Elevating pyrrole derivative synthesis: a three-component revolution. *Mol. Diversity* **2024**, 1−27.
(13) Sidana, N.; Kaur, M.; Kaur, H.; Devi, P. Pyrrole-Based Schiff-Base Sensor for Copper Ions. *ChemistrySelect* **2020**, *5* (46), 14776−14782.
(14) Zhao, C.; Yang, F.; Xia, D.; Zhang, Z.; Zhang, Y.; Yan, N.; You, S.; Li, W. Thieno [3, 4-c] pyrrole-4, 6-dione-based conjugated polymers for organic solar cells. *Chem. Commun.* **2020**, *56* (72), 10394−10408.
(15) Cordell, G. A. 2-Halopyrroles. Synthesis and chemistry. *J. Org. Chem.* **1975**, *40* (22), 3161−3169.
(16) Nguyen, H. Q.; Rainbolt, E. A.; Sista, P.; Stefan, M. C. Synthesis and Polymerization of Fused-Ring Thienodipyrrole Monomers. *Macromol. Chem. Phys.* **2012**, *213* (4), 425−430.
(17) Hendriks, K. H.; Li, W.; Wienk, M. M.; Janssen, R. A. Small-bandgap semiconducting polymers with high near-infrared photoresponse. *J. Am. Chem. Soc.* **2014**, *136* (34), 12130−12136.
(18) Li, Y.; Singh, S. P.; Sonar, P. A high mobility P-type DPP-thieno [3, 2-b] thiophene copolymer for organic thin-film transistors. *Adv. Mater.* **2010**, *22* (43), 4862−4866.
(19) Li, W.; Hendriks, K. H.; Roelofs, W. C.; Kim, Y.; Wienk, M. M.; Janssen, R. A. Efficient small bandgap polymer solar cells with high fill factors for 300 nm thick films. *Adv. Mater.* **2013**, *25* (23), 3182−3186.
(20) Kang, S. H.; Hwang, W. S.; Lin, Z.; Kwon, S. H.; Hong, S. W. A robust highly aligned DNA nanowire array-enabled lithography for graphene nanoribbon transistors. *Nano Lett.* **2015**, *15* (12), 7913−7920.
(21) Karmegam, V.; Udamulle Gedara, C. M.; Biewer, M. C.; Stefan, M. C. Synthesis and opto-electronic properties of functionalized pyrimidine-based conjugated polymers. *J. Polym. Sci., Part A: Polym. Chem.* **2018**, *56* (22), 2547−2553.
(22) Pathiranage, T. M.; Ma, Z.; Udamulle Gedara, C. M.; Pan, X.; Lee, Y.; Gomez, E. D.; Biewer, M. C.; Matyjaszewski, K.; Stefan, M. C. Improved self-assembly of P3HT with pyrene-functionalized methacrylates. *ACS Omega* **2021**, *6* (41), 27325−27334.
(23) Gamage, P. L.; Gunawardhana, R.; Bulumulla, C.; Kularatne, R. N.; Gedara, C. M. U.; Ma, Z.; Biewer, M. C.; Stefan, M. C. An ester functionalized wide bandgap polythiophene for organic field-effect transistors. *Synth. Met.* **2021**, *277*, 116767.
(24) Dissanayake, D. S.; Gunathilake, S. S.; Udamulle Gedara, C. M.; Du, J.; Yoo, S. H.; Lee, Y.; Wang, Q.; Gomez, E. D.; Biewer, M. C.; Stefan, M. C. Conductive triethylene glycol monomethyl ether substituted polythiophenes with high stability in the doped state. *J. Polym. Sci., Part A: Polym. Chem.* **2019**, *57* (10), 1079−1086.
(25) Kline, R. J.; McGehee, M. D.; Kadnikova, E. N.; Liu, J.; Frechet, J. M. Controlling the field-effect mobility of regioregular polythiophene by changing the molecular weight. *Adv. Mater.* **2003**, *15* (18), 1519−1522.
(26) Zen, A.; Pflaum, J.; Hirschmann, S.; Zhuang, W.; Jaiser, F.; Asawapirom, U.; Rabe, J. P.; Scherf, U.; Neher, D. Effect of molecular weight and annealing of poly (3-hexylthiophene) s on the performance of organic field-effect transistors. *Adv. Funct. Mater.* **2004**, *14* (8), 757−764.
(27) Kline, R. J.; McGehee, M. D.; Kadnikova, E. N.; Liu, J.; Fréchet, J. M.; Toney, M. F. Dependence of regioregular poly (3-hexylthiophene) film morphology and field-effect mobility on molecular weight. *Macromolecules* **2005**, *38* (8), 3312−3319.
(28) Zhang, R.; Li, B.; Iovu, M. C.; Jeffries-El, M.; Sauvé, G.; Cooper, J.; Jia, S.; Tristram-Nagle, S.; Smilgies, D. M.; Lambeth, D. N.; et al. Nanostructure dependence of field-effect mobility in regioregular poly (3-hexylthiophene) thin film field effect transistors. *J. Am. Chem. Soc.* **2006**, *128* (11), 3480−3481.
(29) Wang, Y.; Cui, H.; Zhu, M.; Qiu, F.; Peng, J.; Lin, Z. Tailoring phase transition in poly (3-hexylselenophene) thin films and correlating their crystalline polymorphs with charge transport properties for organic field-effect transistors. *Macromolecules* **2017**, *50* (24), 9674−9682.
(30) Himmelberger, S.; Salleo, A. Engineering semiconducting polymers for efficient charge transport. *MRS Commun.* **2015**, *5* (3), 383−395.

(31) Liu, J.; Zhang, R.; Sauvé, G.; Kowalewski, T.; McCullough, R. D. Highly disordered polymer field effect transistors: N-alkyl dithieno [3, 2-b: 2′, 3′-d] pyrrole-based copolymers with surprisingly high charge carrier mobilities. *J. Am. Chem. Soc.* **2008**, *130* (39), 13167−13176.
(32) Bulumulla, C.; Gunawardhana, R.; Kularatne, R. N.; Hill, M. E.; McCandless, G. T.; Biewer, M. C.; Stefan, M. C. Thieno [3, 2-b] pyrrole-benzothiadiazole banana-shaped small molecules for organic field-effect transistors. *ACS Appl. Mater. Interfaces* **2018**, *10* (14), 11818−11825.
(33) Briseno, A. L.; Tseng, R. J.; Ling, M. M.; Falcao, E. H.; Yang, Y.; Wudl, F.; Bao, Z. High-performance organic single-crystal transistors on flexible substrates. *Adv. Mater.* **2006**, *18* (17), 2320−2324.
(34) Kim, Y. H.; Yoo, B.; Anthony, J. E.; Park, S. K. Controlled deposition of a high-performance small-molecule organic single-crystal transistor array by direct ink-jet printing. *Adv. Mater.* **2012**, *24* (4), 497−502.
(35) Goto, O.; Tomiya, S.; Murakami, Y.; Shinozaki, A.; Toda, A.; Kasahara, J.; Hobara, D. Organic Single-Crystal Arrays from Solution-Phase Growth Using Micropattern with Nucleation Control Region. *Adv. Mater.* **2012**, *24* (8), 1117−1122.
(36) Lim, B.; Sun, H.; Lee, J.; Noh, Y.-Y. High performance solution processed organic field effect transistors with novel diketopyrrolo-pyrrole-containing small molecules. *Sci. Rep.* **2017**, *7* (1), 164.
(37) Afzali, A.; Dimitrakopoulos, C. D.; Breen, T. L. High-performance, solution-processed organic thin film transistors from a novel pentacene precursor. *J. Am. Chem. Soc.* **2002**, *124* (30), 8812−8813.
(38) Meng, H.; Zheng, J.; Lovinger, A. J.; Wang, B.-C.; Van Patten, P. G.; Bao, Z. Oligofluorene− thiophene derivatives as high-performance semiconductors for organic thin film transistors. *Chem. Mater.* **2003**, *15* (9), 1778−1787.
(39) Kang, M. J.; Doi, I.; Mori, H.; Miyazaki, E.; Takimiya, K.; Ikeda, M.; Kuwabara, H. Alkylated Dinaphtho [2, 3-b: 2′, 3′-f] Thieno [3, 2-b] Thiophenes (Cn-DNTTs): organic semiconductors for high-performance thin-film transistors. *Adv. Mater.* **2011**, *23* (10), 1222−1225.
(40) Jurchescu, O. D.; Popinciuc, M.; Van Wees, B. J.; Palstra, T. T. Interface-controlled, high-mobility organic transistors. *Adv. Mater.* **2007**, *19*, 688−692.
(41) Takeyama, Y.; Ono, S.; Matsumoto, Y. Organic single crystal transistor characteristics of single-crystal phase pentacene grown by ionic liquid-assisted vacuum deposition. *Appl. Phys. Lett.* **2012**, *101* (8), 083303.
(42) Nenajdenko, V. G.; Sumerin, V. V.; Chernichenko, K. Y.; Balenkova, E. S. A new route to annulated oligothiophenes. *Org. Lett.* **2004**, *6* (20), 3437−3439.
(43) Takimiya, K.; Kunugi, Y.; Konda, Y.; Niihara, N.; Otsubo, T. 2, 6-Diphenylbenzo [1, 2-b: 4, 5-b ‘] dichalcogenophenes: A new class of high-performance semiconductors for organic field-effect transistors. *J. Am. Chem. Soc.* **2004**, *126* (16), 5084−5085.
(44) Pan, H.; Li, Y.; Wu, Y.; Liu, P.; Ong, B. S.; Zhu, S.; Xu, G. Low-temperature, solution-processed, high-mobility polymer semiconductors for thin-film transistors. *J. Am. Chem. Soc.* **2007**, *129* (14), 4112−4113.
(45) Ogawa, K.; Rasmussen, S. C. A simple and efficient route to N-functionalized dithieno [3, 2-b: 2 ‘, 3 ‘-d] pyrroles: Fused-ring building blocks for new conjugated polymeric systems. *J. Org. Chem.* **2003**, *68* (7), 2921−2928.
(46) Gunawardhana, R.; Bulumulla, C.; Gamage, P. L.; Timmerman, A. J.; Udamulle, C. M.; Biewer, M. C.; Stefan, M. C. Thieno [3, 2-b] pyrrole and Benzo [c][1, 2, 5] thiadiazole Donor−Acceptor Semiconductors for Organic Field-Effect Transistors. *ACS Omega* **2019**, *4* (22), 19676−19682.
(47) Bulumulla, C.; Kularatne, R. N.; Gunawardhana, R.; Nguyen, H. Q.; McCandless, G. T.; Biewer, M. C.; Stefan, M. C. Incorporation of thieno [3, 2-b] pyrrole into diketopyrrolopyrrole-based copolymers for efficient organic field effect transistors. *ACS Macro Lett.* **2018**, *7* (6), 629−634.
(48) Bulumulla, C.; Gunawardhana, R.; Yoo, S. H.; Mills, C. R.; Kularatne, R. N.; Jackson, T. N.; Biewer, M. C.; Gomez, E. D.; Stefan, M. C. The effect of single atom replacement on organic thin film transistors: case of thieno [3, 2-b] pyrrole vs. furo [3, 2-b] pyrrole. *J. Mater. Chem. C* **2018**, *6* (37), 10050−10058.
(49) Usta, H.; Lu, G.; Facchetti, A.; Marks, T. J. Dithienosilole− and dibenzosilole− thiophene copolymers as semiconductors for organic thin-film transistors. *J. Am. Chem. Soc.* **2006**, *128* (28), 9034−9035.
(50) Gamage, P. L.; Udamulle Gedara, C. M.; Ma, Z.; Bhadran, A.; Gunawardhana, R.; Bulumulla, C.; Biewer, M. C.; Stefan, M. C. Incorporation of Selenopheno [3, 2-b] pyrrole into Benzothiadiazole-Based Small Molecules for Organic Field-Effect Transistors. *ACS Appl. Electron. Mater.* **2021**, *3* (12), 5335−5344.
(51) Zhang, M.; Tsao, H. N.; Pisula, W.; Yang, C.; Mishra, A. K.; Müllen, K. Field-effect transistors based on a benzothiadiazole−cyclopentadithiophene copolymer. *J. Am. Chem. Soc.* **2007**, *129* (12), 3472−3473.
(52) Gamage, P. L.; Udamulle Gedara, C. M.; Gunawardhana, R.; Bulumulla, C.; Ma, Z.; Shrivastava, A.; Biewer, M. C.; Stefan, M. C. Enhancement in Charge Carrier Mobility by Using Furan as Spacer in Thieno [3, 2-b] Pyrrole and Alkylated-Diketopyrrolopyrrole Based Conjugated Copolymers. *Appl. Sci.* **2022**, *12* (6), 3150.
(53) Maeda, T.; Tsukamoto, T.; Seto, A.; Yagi, S.; Nakazumi, H. Synthesis and Characterization of Squaraine-Based Conjugated Polymers With Phenylene Linkers for Bulk Heterojunction Solar Cells. *Macromol. Chem. Phys.* **2012**, *213* (24), 2590−2597.
(54) Bronstein, H.; Hurhangee, M.; Fregoso, E. C.; Beatrup, D.; Soon, Y. W.; Huang, Z.; Hadipour, A.; Tuladhar, P. S.; Rossbauer, S.; Sohn, E.-H.; et al. Isostructural, deeper highest occupied molecular orbital analogues of poly (3-hexylthiophene) for high-open circuit voltage organic solar cells. *Chem. Mater.* **2013**, *25* (21), 4239−4249.

https://doi.org/10.1021/acsomega.4c11362
ACS Omega 2025, 10, 12357−12365